European Journal of Medicinal Chemistry 80 (2014) 1–7

Contents lists available at ScienceDirect

European Journal of Medicinal Chemistry

journal homepage: http://www.elsevier.com/locate/ejmech

Original article

Synthesis, cytotoxicity for mimics of catalase: Inhibitors of lactate dehydrogenase and hypoxia inducible factor

Juan-Juan Xue [a], Qiu-Yun Chen [a,*], Meng-Yun Kong [a], Chun-Yin Zhu [a], Zhi-Rong Gen [b], Zhi-Lin Wang [b]

[a] School of Chemistry and Chemical Engineering, Jiangsu University, Zhenjiang 212013, PR China
[b] State Key Laboratory of Coordination Chemistry, Nanjing University, Nanjing 210093, PR China

ARTICLE INFO

Article history:
Received 31 October 2013
Received in revised form
12 March 2014
Accepted 10 April 2014
Available online 13 April 2014

Keywords:
Mimics of catalase
Cancer cells
LDH
HIF
Manganese

ABSTRACT

Lactate dehydrogenase A (LDH-A) is a potentially important metabolic target for the inhibition of the highly activated glycolysis pathway in cancer cells. Two Mn(II) complexes with ligand containing di(pyridylmethyl) amine and pyrrol-ketone were used to attenuate the activity of LDH-A. The inhibition of the manganese(II) complexes on the proliferation of HepG-2 cells is related to their ability to disproportionate H_2O_2. Importantly, the synthesized mimic of catalase can decrease the expression of hypoxia inducible factor (HIF-1α) in HepG-2 cells. So we envision that the multifunctional mimics of catalase could attenuate the activity of LDH-A signaling the cancer cells to death through HIF-1α involved path.

1. Introduction

Cancer cells typically display altered glucose metabolism characterized by a preference of aerobic glycolysis, known as the Warburg effect, which facilitates cell proliferation [1]. Glycolysis allows for continued ATP production without the need of O_2-dependent oxidative phosphorylation, and is thus an important pathway under hypoxic conditions [2]. Altered cancer cell energy metabolism has been categorized as an emerging hallmark of cancer, and thus, inhibition of metabolic processes associated with cancer cell growth constitutes a promising approach in the search for new cancer therapies [3,4]. One molecular target in the glycolytic pathway is the lactate dehydrogenase (LDH) which catalyzes the interconversion of lactate and pyruvate [5,6]. In mammalian cells, there are four major isoforms of LDH, LDH-A, LDH-b, LDH-c and LDH-h, with the A form having higher intrinsic activity to catalyze the transformation of pyruvate to lactate. LDH-A is a potentially important metabolic target for inhibition of the highly activated glycolysis pathway in cancer cells [7]. Most reported LDH-A inhibitors, such as oxamate, 3-hydroxyisoxazole-4-carboxylic acid and N-hydroxyindole, are competitive with the pyruvate or NADH substrate binding [7–9]. Moreover, targeted inhibition of HIF-1α is another new pathway to cancer therapy. Hypoxia-inducible factor (HIF-1α) regulates the energy metabolism by triggering a switch from mitochondrial oxidative phosphorylation to anaerobic glycolysis, increasing the expression of genes that encode glycolytic enzymes and glucose transporters [10]. Cancer cells activate glycolysis to meet their energy demands and use O_2 to generate excessive levels of the reactive oxygen species (ROS), superoxide anion ($O_2^{\cdot-}$) and hydrogen peroxide (H_2O_2). H_2O_2, a kind of ROS generated in mitochondria, is considered a mediator of apoptotic cancer cell, and can be eliminated by mitochondrial catalase [11,12]. With the over-expression of H_2O_2-detoxifying enzymes or human catalase *in vivo*, H_2O_2 concentration will decrease, and cancer cells could revert to normal appearance [13]. Thus, H_2O_2 is also an important signal molecule to attenuate the metabolite of oxygen in cancer cells and the catalase could be a modulator of HIF-1α signals.

It is reported that the manganese(III) porphyrin complexes could decrease the mitochondrial H_2O_2 [14]. Previously we found that the carboxylate-bridged dimanganese(II) systems could be used as functional models of catalase, which could inhibit the

Abbreviations: LDH-A, Lactate dehydrogenase; HIF, hypoxia inducible factor; dpa, Di(pyridine-2-yl)methyl)amine; PPMdpa, 4-(Chloromethyl)phenyl)(3,5-dimethyl-1*H*-pyrrol-2-yl)methanone); pydpa, *N*-(3-Pyridyl)methyl-di(pyridylmethyl)amine; phdpa, *N*-Benzyl-di(pyridylmethyl)amine; Mn1, [(PPMdpa)$MnCl_2$]; Mn2, [(PPMdpa)$MnAc_2$]; Hepes, 4-(2-Hydroxyethyl)-1-pierazineethanesulfonic acid; DMEM, Dulbecoo's modified Eagle's medium.

* Corresponding author.
E-mail address: chenqy@ujs.edu.cn (Q.-Y. Chen).

http://dx.doi.org/10.1016/j.ejmech.2014.04.035
0223-5234/

proliferation of HeLa cells through ROS signal induced apoptosis [15]. These lipophilic complexes can accumulate in cancer cells through perturbing the mitochondrial membrane potential or inhibiting the swelling of over calcium(II) loaded mitochondria [16,17]. Thus, we propose that the conjugation of pyrrol-conjugated C═O groups (3,5-dimethyl-1H-pyrrole-2-carbonyl portion, Scheme 1 and Scheme S1) with Mn(II) complexes of di(picolyl) amine would produce a new kind of multifunctional complexes with activity of inhibiting LDH-A and HIF-1α. Here, we report the synthesis, characterization and bioactivities of Mn(II) complexes of PPMdpa.

2. Results and discussion

2.1. Synthesis and characterization of ligand (PPMdpa) and complexes

Di(pyridine-2-ylmethyl)amine (dpa) and 4-(chloromethyl) phenyl)(3,5-dimethyl-1H-pyrrol-2-yl)methanone (PPM) were refluxed in acetonitrile under nitrogen producing PPMdpa in 66% yield (Scheme S1). The ^{1}H NMR spectra of the PPM and PPMdpa confirm the existence of PPMdpa (Figs. S1 and S2). Subsequent reaction of PPMdpa with $MnCl_2{\cdot}4H_2O$ or $MnAc_2{\cdot}6H_2O$ resulted in the formation of complexes Mn1 or Mn2. The structures of complexes Mn1 and Mn2 were characterized by elemental analyses, IR, UV, ES-MS and EPR. The elemental analyses show that the ratio of metal:L in all complexes is 1:1. The PPMdpa and Mn1 are unsoluble in water, while Mn2 is slightly soluble in water. The δ(CH) vibration of pyridyl ring is at approximately 760 cm^{-1} [18]. In contrast, these vibrations in the complexes Mn1 and Mn2 are all shifted to 762 and 765 cm^{-1}, respectively. These shifts can be explained by the fact that the nitrogen atoms of pyridyl ring of the ligands donate a pair of electrons each to the central metal ions, forming coordinate covalent bond [19]. The ν(C═O) bands of the complexes Mn1 and Mn2 appear at approximately 1610 cm^{-1} and 1606 cm^{-1}, respectively, indicating the existence of the pyrrol-conjugated carbonyl group in PPMdpa (Fig. S3) [20]. The strong peak at 3237 cm^{-1} for Mn1 and Mn2 in infrared spectra was assigned to ν(N–H) stretching frequencies showing the existence of pyrrole in PPMdpa. The stretching frequencies of ν (COO^-) at 1570 cm^{-1} and 1016 cm^{-1} for complex Mn2, indicates the existence of COO^- [21].

The UV spectra of PPMdpa had bands at 206, 248 and 323 nm (Fig. S4 and Table S1). The band at 248 nm can be attributed to the n–π* transition of the pyrrole-conjugated C═O. This band for complexes Mn1 and Mn2 was red shift to 257 nm and 256 nm, respectively. Nearly no free Mn(II) ions could be measured for the solution of Mn1 and Mn2 in water-DMSO (1:1) by ICP methods, indicating Mn1 and Mn2 are stable in solution. The main peak for PPMdpa m/z = 411.36(100) corresponds to species $[(PPMdpa)H]^+$ indicating that the PPMdpa is stable in the ES-MS condition (Fig. S5). The main peak for Mn2 at m/z = 524.29 (100) corresponds to species $[(PPMdpa)Mn(\mu\text{-}Ac)_2Mn(PPMdpa)]^{2+}$, which indicates the existence of Mn2 (Fig. S6). The 50.58% weight loss in the range of 109–540 °C corresponds to the loss of di(pyridylmethyl)amine groups from the ligand and two chlorine ions in Mn1 (calcd 50.37%) (Fig. S7A). Thermal analysis (TG) curves of Mn2 in the range of temperature from 0 to 1000 °C are shown in Fig. S7B. The weight loss of 54.25% at 98–460 °C for Mn2 is attributed to the loss of four Ac^- ions and two dpa groups from the ligand (calcd 54.37%). Thermal analysis results confirm the formation of $[(PPMdpa)Mn(\mu\text{-}Ac)_2Mn(PPMdpa)Ac_2]$ (Mn2). The paramagnetic resonance of the powder solid state complex Mn2 was carried out at 110 K. The EPR spectrum recorded for the Mn2 displays a strong signal centered at g = 2.01 with no hyperfine splitting indicating no Mn–Mn coupling interaction in Mn2, which is consistent with that of those reported dimanganese(II) species (Fig. S8) [22].

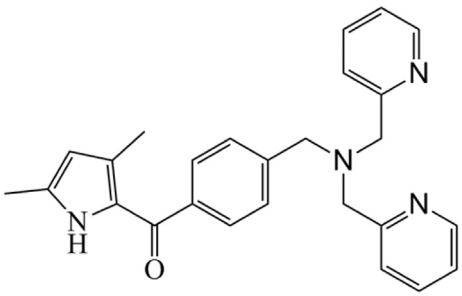

PPMdpa

Scheme 1. The chemical structure of PPMdpa.

2.2. Crystal structure of $[(PPMdpa)_2Mn_2(\mu\text{-}Cl)_2Cl_2]_2$ (Mn1)

The molecular structure of $[(PPMdpa)_2Mn_2(\mu\text{-}Cl)_2Cl_2]_2$ (Mn1) with the atomic labeling scheme is shown Fig. 1, and the selected bond lengths and angles are listed in Table S3. The Mn1 atom in $[(PPMdpa)_2Mn_2(\mu\text{-}Cl)_2Cl_2]_2$ (Mn1) is coordinated by three N atoms (N2, N3, N4), one chloride atom (Cl1), and two bridged chloride anions (Cl2, Cl2A), resulting in a six coordinate dinuclear Mn(II) complex. The complex $[(PPMdpa)_2Mn_2(\mu\text{-}Cl)_2Cl_2]_2$ thus shows a distorted octahedral geometry. Atoms N2, N3, Cl2 and Cl2A form the equatorial tetragonal plane (mean deviation = 0.0828), while N4 and Cl1 occupy the apical positions. The Mn1 atom is shifted by 0.3419 Å out of the equatorial plane toward Cl2. The Mn1–N4 and Mn1–Cl1 bond distances are 2.387(3) and 2.4257(13) Å, respectively. The N4–Mn1–Cl1 angle is 159.28(9) Å. Atoms N2A, N3A, Cl2 and Cl2A form the equatorial tetragonal plane (mean deviation = 0.0828), while N4A and Cl1A occupy the apical positions. The Mn1A atom is shifted by 0.3419 Å out of the equatorial plane toward Cl2. The Mn1–N4 and Mn1–Cl1 bond distances are 2.387(3) and 2.4257(13) Å, respectively. The N4–Mn1–Cl1 angle is 159.28(9) Å.

2.3. Catalase-like activity measured by O_2 evolution – kinetics studies

The progresses of the reactions between complexes and H_2O_2 at various conditions were monitored by UV–vis spectroscopy. When H_2O_2 (0.5 mL, 30%) was added to the white-yellow solution of Mn2, the color of the solution became dark-yellow and poorly resolved absorption bands in the range of 400–800 nm appeared, which indicate that complex Mn2 could bind with H_2O_2 (Fig. S9). The O_2 evolution volume was used for the kinetic study of H_2O_2 disproportionation. The H_2O_2 disproportionation promoted by complexes was carried out in MeCN and buffered solutions ((Tris/Tris–HCl 0.1 M, NaCl 0.1 M, pH 7.4) at 0 and 37 °C. It was found that less gas evolution could be monitored when Mn1 was incubated with H_2O_2, even after 3 h under the conditions described above, demonstrating that Mn1 could not catalyze the disproportionation of dihydrogen peroxide (Fig. 2a). In contrast, complex Mn2 can disproportionate dihydrogen peroxide to generate dioxygen. The complex Mn2 could disproportionate 0.5 mL H_2O_2 aqueous to liberate 1 mmol O_2. The obtained plot of the initial rate vs the concentration of dihydrogen peroxide is fitted by using the Hill equation ($V_0 = V_{max}\ [s]^n/(K_m + [s]^n)$) (Fig. S10, Fig. S11). The parameter K_{cat} is calculated from the equation $K_{cat} = V_{max}/[E_t]$ [23,24]. The maximum O_2 evolution rates were about 4.74 mM s^{-1} and 0.94 mM s^{-1} for Mn2 in the MeCN and Tris–HCl solution, respectively. The Hill constants (n)

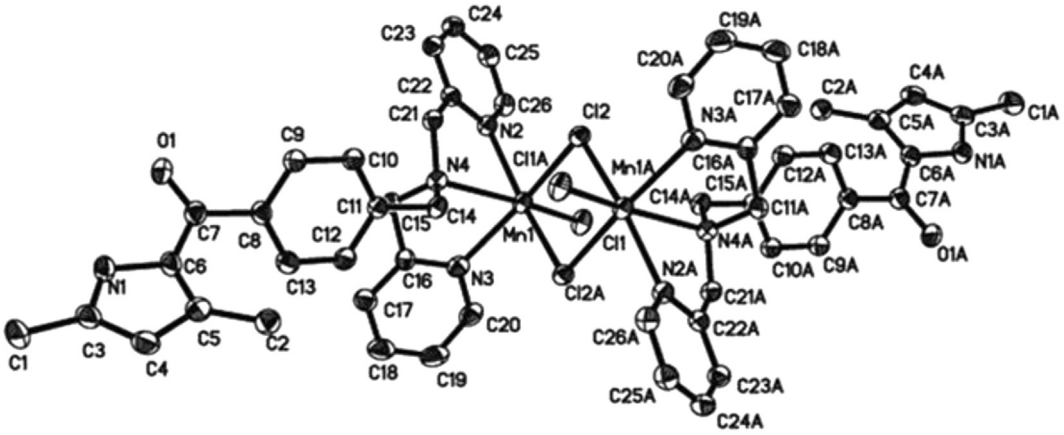

Fig. 1. Crystal structure of $[(PPMdpa)_2Mn_2(\mu\text{-}Cl)_2Cl_2]_2$ (Mn1). Hydrogen atoms were omitted.

and turnover number K_{cat} for Mn2 in both MeCN and buffered solutions are 1.46 ± 0.3 and 2.86 ± 0.2, and 9.95 and 1.40, respectively (Table S4). The turnover numbers of Mn2 in MeCN was higher than that of $[(Adpa)Mn(\mu_2\text{-}O)_2Mn(Adpa)]PF_6 \cdot 8H_2O$, $[(Adpa)_2Mn_2(Ac)(H_2O)_2](Ac)$ and $[TPA_2Mn_2(\mu\text{-}O)_2](ClO_4)_3$ but was lower than that of manganese complexes with bpia ligand and N,N′-bis(3-selenomethyl-salicyladehyde-5-sulfonate) bis(1,3)-diamino-2-hydroxypropane) Schiff base [25,26]. Though the two characterized manganese catalases *Thermus thermophilus catalase* and *Thermoleophilum album catalase* showed much higher catalytic activity for the disproportionation of dihydrogen peroxide than Mn2, the activities of the synthetic mimics (Mn2) of catalase were remarkable [27–29]. According to the results, the intrinsic H_2O_2 disproportionation activities of complexes were in the order Mn2 >> Mn1. The catalase activity of Mn2 under different conditions is shown in Fig. 2b. The condition of the reaction carried out at 37 °C in Tris–HCl solution was the mimetic condition of the cell environment. Thus, we deduce that complex Mn2 would also show good catalase activity in vitro.

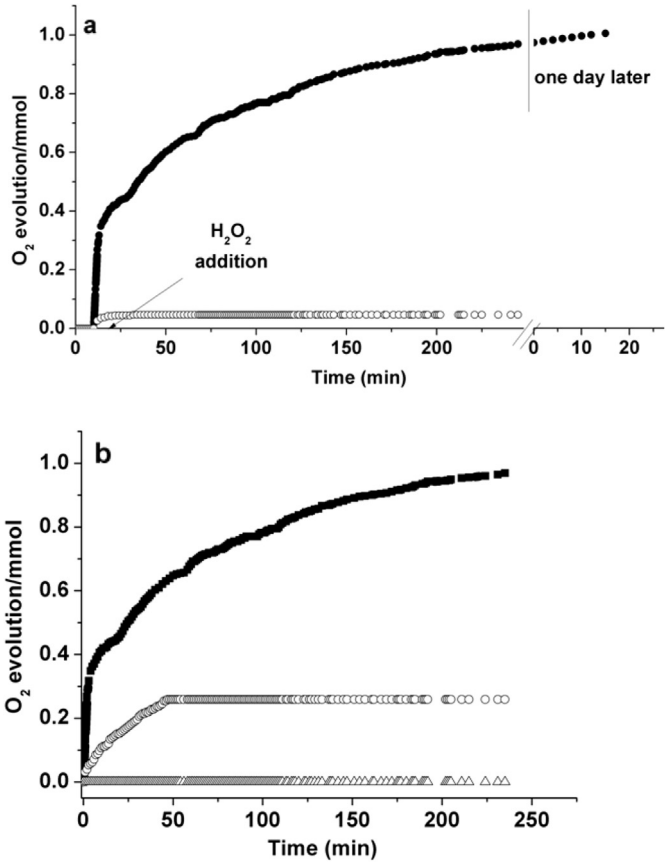

Fig. 2. (a) Rates of the O_2 evolution of the complexes at 37 °C in MeCN, $C_{complexes}$ = 0.5 mM, 0.5 mL of 30% H_2O_2 aqueous solution, V_{MeCN} = 3 mL Mn1 (○), Mn2 (■). (b) Rates of the O_2 evolution of the complex Mn2 at different conditions, C_{Mn2} = 0.5 mM, 0.5 mL of 30% H_2O_2 aqueous solution, $V_{solvent}$ = 3 mL. 37 °C in MeCN (■), 37 °C in Tris–HCl (○), 0 °C in Tris–HCl (△).

2.4. Evaluation of enzyme activity for inhibitors of LDH-A

The LDH inhibitory activities of the new compounds were measured by standard enzyme kinetic experiments on rabbit LDH-A purified isoform [8]. Initially, we verified the percentage inhibition relative to control at 30–120 μM for all compounds with LDH-A (Fig. 3). It is observed that the inhibiting effect for the compounds is dependent on the concentration. We were pleased to find a dramatic increase in the LDH-A inhibition level when the concentration increase to 75 μM, with a 10% PPMdpa, a 60% Mn2 and a 99% Mn1 inhibition, respectively. However, previously reported Mn(II) complex $[(phdpa)_2Mn_2(\mu\text{-}Cl)_2(Cl)_2]$ [15] (75 μM) have no inhibition on the activity of LDH-A in the same condition (Table S5). The difference between $[(phdpa)_2Mn_2(\mu\text{-}Cl)_2(Cl)_2]$ and Mn1 is that

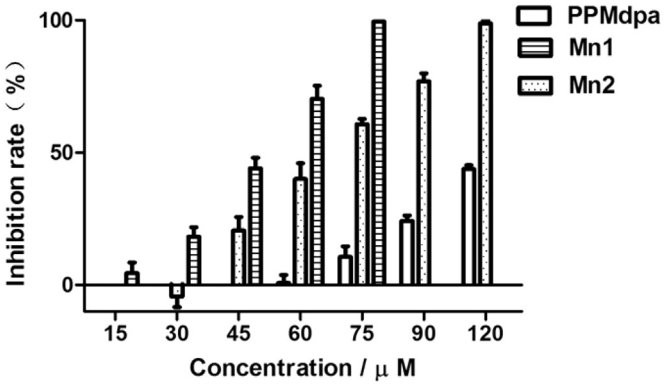

Fig. 3. Colorimetric measurement of inhibition (% relative to control) of the enzymatic activity of LDH-A in the presence of PPMdpa, Mn1 and Mn2 (concentration were PPMdpa and Mn1 and Mn2). Values are reported as the mean ± the SD of three independent experiments, the SD < 0.05.

there are pyrrol-conjugated C=O groups in Mn1, so we deduce that pyrrol-conjugated C=O groups (3,5-dimethyl-1H-pyrrole-2-carbonyl portion) give great contribution to the inhibition for Mn1 to LDH-A. The apparent Michaelis–Menten constants (K_m) of NADH and pyruvate for LDH-A were measured by Lineweaver–Burk plots. From the values of K'_m so obtained, K_i values for each single inhibitor were determined using double-reciprocal Lineweaver–Burk plots (Fig. 4, Table 1). For Mn2, K_i value is 41.7 μM vs NADH and 21.4 μM vs pyruvate. Therefore, we deduce that both compounds were found to be more competitive inhibitors of LDH-A with respect to NADH than pyruvate in the conversion of pyruvate to lactate catalyzed by this enzyme, whereby NADH is converted to NAD^+.

2.5. Cytotoxicity assay and effect on the expression of HIF-1α

The in vitro cytotoxicity of complexes (Mn1 and Mn2) was evaluated using MTT assay by measuring anti-proliferation on HepG-2 cells. 5-Fluorouracial was used as a positive control for cytotoxicity. The IC_{50} values are shown in Table 2. Complexes Mn1 and Mn2 can inhibit the proliferation of the HepG-2 cells with IC_{50} 0.95 and 2.59 μM. These indicate Mn1 and Mn2 are more active than previous reported Mn(II) complexes $[(pydpa)_2Mn_3(H_2O)_2(Cl_6)]$ and $[(phdpa)_2Mn_2(\mu\text{-}Cl)_2(Cl)_2]$ [15]. The inhibiting

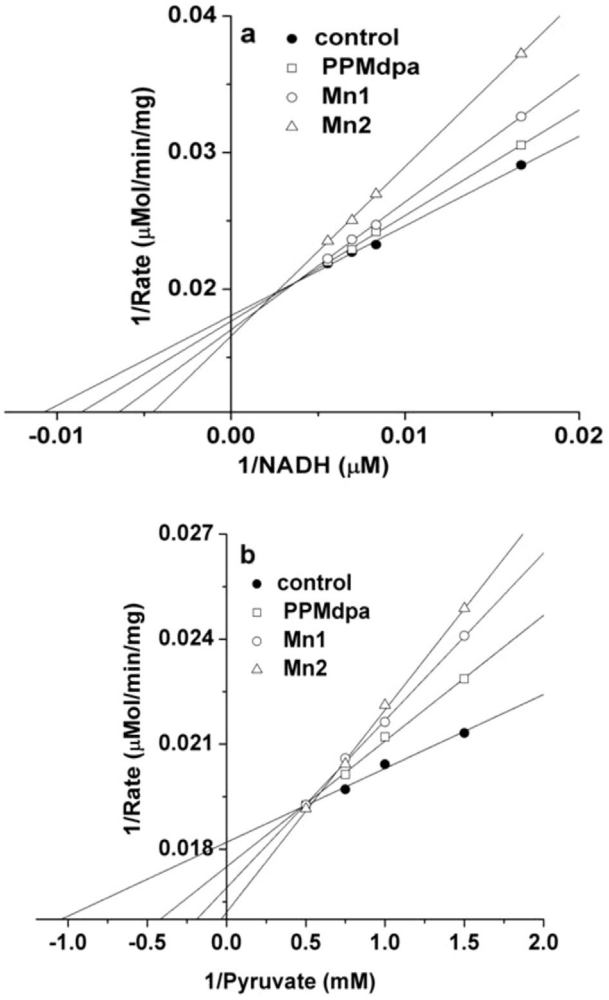

Fig. 4. Lineweaver–Burk plots determined from triplicate experiments with inhibitors PPMdpa (90 μM), Mn1 (45 μM) and Mn2 (45 μM) using average activities: competition experiments with NADH (a) and pyruvate (b).

Table 1
Inhibition data (K_i for LDH-A) obtained with Compounds.[a]

Compound	LDH-a (K_i, μM)	
	[NADH][b]	[Pyruvate][c]
PPMdpa	414.9 ± 1.7	114.9 ± 1.5
Mn1	85.7 ± 1.3	30.9 ± 2.6
Mn2	41.7 ± 2.3	21.4 ± 0.7

[a] K_i determination was performed in presence of compounds PPMdpa, Mn1 and Mn2 as described in the Experimental Section. Values are reported as mean ± SD of three or more independent experiments.
[b] Saturating concentration (2 mM) of pyruvate and competitive increasing concentrations (60–180 μM) of NADH.
[c] Saturating concentration (180 μM) of NADH and competitive increasing concentrations (0.67–2 mM) of pyruvate.

effects for Mn1 and Mn2 on HepG-2 cells are dependent on their concentration (Fig. S12 and Fig. 5). The anticancer property, good solubility and mimic of catalase make Mn2 a potential multifunctional complex. The inhibiting rate of Mn2 is slightly smaller than that of Mn1 in 24 h. This indicates that H_2O_2 discriminating properties may have some effect on the metabolite of oxygen or the ROS signaling apoptosis in cancer cells. Oxygen is an important factor to maintain cell life and the final electron acceptor in oxidative phosphorylation for energy production [30]. Hypoxia-inducible factor (HIF) regulates the energy metabolism by triggering a switch from mitochondrial oxidative phosphorylation to anaerobic glycolysis, increasing the expression of genes that encode glycolytic enzymes and glucose transporters [31]. HIF is a common link between O_2 availability, malignant progression, and changes in cancer metabolism. Mn2 is a good mimic of catalase and inhibitor of LDH-A, it may have some effect on the expression of HIF-1α in HepG-2 cells. Experimental results show that the Mn2 obviously decreases the expression of HIF-1α in 24 h (Fig. 6). Therefore, this result demonstrates that Mn2 is a multifunctional complex to attenuate the expression of HIF-1α in cancer cells.

3. Conclusion

Mn(II) complexes with (4-((bis(pyridin-2-lmethyl)amino) methyl) phenyl)(3,5-dimethyl-1H-pyrrol-2-yl) methanone (PPMdpa) were characterized and used as mimics of catalase and inhibitors of LDH-A. This is the first report that functional mimics of catalase (Mn(II) complexes) can be as inhibitor of LDH-A. The anticancer activity of Mn2, a good mimic of catalase, is smaller than that of Mn1, demonstrating that the inhibition of these manganese(II) complexes on tumor cells in vitro is related to their H_2O_2 disproportionating activity. Importantly, Mn2 can decrease the expression of HIF-1α in HepG-2 cells. Therefore, Mn2 can be used as a chemical sensitizer to explore the cross-talk mechanism of HIF-1α related oxygen and energy metabolism in cancer cells in the future. Given these advantages, we envision that combination of potential inhibitors of LDH-A and mimics of catalase would promote the development of compounds that can attenuate the metabolism of oxygen and energy signaling the cancer cells to death through HIF-1α involved path.

4. Experimental

4.1. General methods

The C, H and N microanalyses were performed on Vario EL elemental analyzer. The electronic absorption spectra were recorded in the 200–800 nm regions using a Varian Cary 50-BIO UV–vis spectrophotometer. The IR spectra were recorded on a Nicolet-470

Table 2
IC_{50} values of the complexes on HepG-2 cell lines.

Complex	HepG-2
Mn1	0.95 ± 0.2
Mn2	2.59 ± 0.3
PPMdpa	21.5 ± 0.3
$MnCl_2$	>100
5-Fluorouracil**	32 ± 0.8

*All IC_{50} values were expressed as mean values of the three experiments. **5-Fluorouracil was used as a positive control.

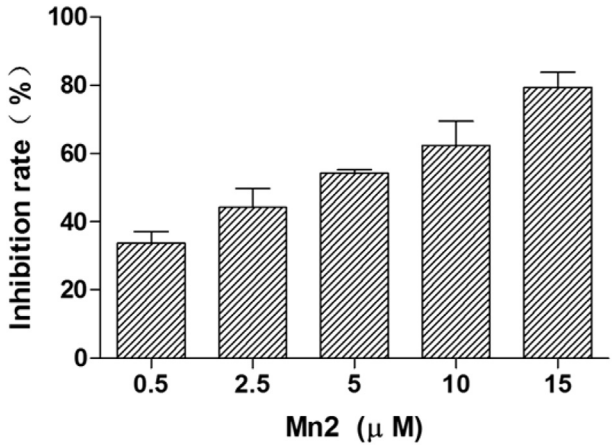

Fig. 5. The concentration dependence of Mn2 on HepG-2 cells. Cell proliferation was determined by MTT assay every 12 h. Each column represents the mean of the data from three independent experiments.

spectrophotometer in the range 4000–400 cm^{-1}. The 1H NMR spectra were measured on a Bruker 400 MHz spectrometer. The electrospray mass spectra (ES-MS) were determined on a Finnigan LCQ mass spectrograph, and the concentration of samples was about 1.0 μmol L^{-1}. The diluted solution was electrosprayed at a flow rate of 5×10^{-6} L^{-1} min^{-1} with a needled voltage of +4.5 kV. The mobile phase was methanol. X-band EPR spectra were recorded on a Bruker BioSpin GmbH instrument in liquid nitrogen (110 K).

4.2. X-ray crystal structure determination

Crystallographic data for $[(PPMdpa)_2Mn_2(\mu\text{-}Cl)_2Cl_2]_2$ (Mn1) is listed in Table S2. The crystal of the complex was selected for lattice parameter determination and collection of intensity data at 293 K on a Rigaku Mercury2 CCD area detector (MSC Inc., 2005) with monochromatized Mo Kα radiation ($\lambda = 0.71073$ Å). The data was corrected for Lorenz and polarization effects during the data reduction. A semiempirical absorption correction from equivalents

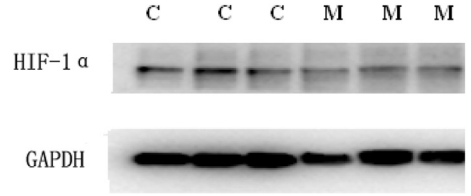

Fig. 6. The expression of HIF-1α in HepG-2 cells after incubated with Mn2 (M) (2.6 μM) for 24 h. Control (C) (10 μM DMSO). (The experiment was repeated for three times).

was applied on the basis of multiscan. The structure was solved by direct methods and refined on F^2 by the full-matrix least-squares methods, using SHELXTL version 5.10 [32]. All non-hydrogen atoms were refined anisotropically. Hydrogen atoms were introduced in their calculated positions. All computations were carried out using the SHELXTL-PC program package.

4.3. Catalase-like activity

All of the reactions between the complexes and dihydrogen peroxide were performed in buffered (Tris/Tris–HCl 0.1 M, NaCl 0.1 M, pH 7.4) at 0 and 37 °C. The reactivity of the complexes with H_2O_2 was first investigated in water via UV–vis spectroscopy titration at 37 °C. After the solution (10 mL) of complexes (0.5 mM) was stirred at 37 °C for 30 min, 0.5 mL of H_2O_2 aqueous solution (30%) was added, and the spectra were recorded at 5 min intervals at 37 °C. The volumetric measurements of the evolved dioxygen produced during the reaction of the complexes with H_2O_2 were performed in triplicate as follows: a 25 mL round-bottom flask containing a complex (0.5×10^{-3} M, 3.0 mL) in MeCN solvent (or a buffered system) was placed in an ice (0 ± 0.1 °C) bath. The flask was closed with a rubber septum, and a cannula was used to connect the reaction flask to an inverted graduated pipet, filled with water. While the solution containing the complex was being stirred, a solution of 0.5 mL of H_2O_2 aqueous solution was added through the septum using a microsyringe. The volume of oxygen produced was measured in the pipet. The kinetics measurements of complexes, Mn1 and Mn2 were performed in MeCN solution at 37 °C. Different concentrations of dihydrogen peroxide were prepared by diluting the 30% H_2O_2 aqueous solution with acetonitrile solution or Tris–HCl buffer solution. The optimum reaction order of the substrate with respect to the complexes was determined by reacting different concentrations of complexes with a constant concentration of substrate. Similarly, the optimum reaction order of the complexes with respect to the substrate was determined by reacting different concentrations of substrate with a constant concentration of complexes.

4.4. Inhibition of lactate dehydrogenase

Lactate dehydrogenase (LDH-A), an enzyme is the glycolysis pathway, is considered a significant small-molecule oncology target in cancer metabolism. The oxidation of NADH is observed at 340 nm, which is a direct measure of the reduction of pyruvate to lactate in the absence of interfering reactions. The apparent Michaelis–Menten constants (K_m) of LDH-A was measured from Lineweaver–Burk plots. The reaction velocity of purified LDH-A was determined by a decrease in absorbance at 340 nm of NADH, and the value of optical density was determined at 30 s intervals for 4 min. LDH-A activity was determined at 37 °C by measuring the oxidation of NADH spectrophotometrically at 340 nm as a function of time. The K_m values of LDH-A for NADH and pyruvate were determined in saturating conditions as described below. In 100 mM sodium phosphate buffer (pH 7.4), 0.5 units of LDH-A were combined with 2 mM pyruvate (pyruvate-saturated) and 60–180 μM NADH, or 180 μM NADH (NADH-saturated) and 0.67 mM–2 mM pyruvate. These conditions were used for all assays. The reaction velocity of LDH was determined spectrophotometrically (UV–vis spectrophotometer) by a decrease in absorbance at 340 nm ($\varepsilon = 6.2$ mM^{-1} cm^{-1}) of NADH. Michaelis–Menten constants for substrates were determined from initial rate measurements at 37 °C by nonlinear regression analysis with the Origin 8.0. Under these conditions NADH showed a Km of 36 μM and a V_{max} of 55 (μmol/min)/mg, whereas the pyruvate showed a K_m of 115 μM and a Vmax of 55 (μmol/min)/mg. Compounds PPMdpa, Mn1 and Mn2

were dissolved in stock solutions of DMSO (concentrations of DMSO during the initial rate measurements did not exceed 0.5%). Using 180 μM NADH and 2 mM pyruvate, we initially evaluated the percent inhibition of the compounds. We evaluated the apparent K'_m values in the presence of inhibitors. From the values of K'_m so obtained, K_i values for each single inhibitor were determined using double–reciprocal plots [33].

4.5. Cytotoxicity testing

The cytotoxicity assay was in one kind of HepG-2 cells. Cells were cultured in RMPI 1640 medium containing 4.8 g/L of Hepes, 2.2 g/L $NaHCO_3$ and supplemented *i*th penicillin/streptomycin (1000 units/ml), and 10% calf serum. HepG-2 cells were cultured in DMEM medium containing 10% fetal bovine serum. All cells were grown at 37 °C in a humidified atmosphere in the presence of 5% CO_2. HepG-2 cells were seeded at a density of 4 × 104 cells/mL into sterile 96-well plates and grown in 5% CO_2 at 37 °C. Test compounds were dissolved in DMSO and diluted with culture media. After 24 h, compounds were added, treated for 48 h. Cell viability was determined by the 3-[4,5-dimethylthiazol-2-yl]-2,5-diphenpyltetrazolium bromide (MTT) assay by measuring the absorbance at 570 nm with ELISA reader. IC_{50} data are calculated by the software provided by Nanjing University. All experiments were repeated at least three times.

4.6. Western blot analysis on expression level of HIF-1α in HepG-2 cells

Nuclear protein extracts were prepared from 100 mm dishes, except for experiments performed on 60 mm gas permeable dishes (Greiner Bio One, Frickenhausen, Germany), protein was isolated to perform Western analysis on Mini-Proten Tetra System (Molecular Devices, Bio-RAD). A monoclonal mouse antibody for human HIF-1α (2015-1, Epitomics) and a monoclonal mouse GAPDH Antibody (AP0063, Bioworld) were used. Horseradish peroxidase-conjugated goat anti-rabbit IgG-HRP: (BS13278, Bioworld) was used as secondary antibodies. Image was performed using ChemiDoc XRS + System (Bio-RAD).

4.7. Chemicals and starting materials

Bis(pyridine-2-ylmethyl)amine (dpa, purity 99%), Tris (tris(hydroxymethyl)amino-methane) (tris), LDH-A, NADH, pyruvate, 4-(chloromethyl)benzoyl chloride and 4-dimethyl-1H-pyrrole were purchased from Sigma–Aldrich. All chemicals used for synthesis were of reagent grade and used without further purification (Sinopharm Chemical Reagent Co. Ltd., China). Water was purified with a Millipore Milli-Q system. Column chromatography was carried out using silica FCP (200–300 mesh).

4.8. Synthesis of (4-(chloromethyl)phenyl)(3,5-dimethyl-1H-pyrrol-2-yl)methanone (PPM)

4-(Chloromethyl)benzoyl chloride (1.5 g, 7.9 mmol) and triethyl amine (1.061 g, 10.51 mmol) were dissolved in dichloromethane (40 mL) under nitrogen at 0 °C, then 2,4-Dimethyl-1*H*-pyrrole (523 mg, 25 mmol) was added. After that, the mixture was stirred for 6 h at room temperature; the solution was washed with 1 M NaCl (20 mL) solution, dried with sodium sulfate and concentrated to give oil liquid. After column chromatography on silica gel, light yellow powder 4-(Chloromethyl)phenyl)(3,5-dimethyl-1H-pyrrol-2-yl)methanone was obtained. Yield: 668 mg (70%); elemental analysis calcd (%) for $C_{14}H_{14}ClNO$: C, 67.88; H, 5.7; N, 5.65. Found: C, 67.58; H, 5.32; N, 5.85; IR (KBr, ν/cm^{-1}): ν = 3230 (=NH), 1611 (C=O). ^1H NMR ($CDCl_3$, 400 MHz, 25 °C, TMS), δ = 9.54 (s, 1H; pyrrole, N–H); 7.65 (d, J = 8.0 Hz, 2H; BzH); 7.48 (d, J = 8.0 Hz, 2H; BzH); 5.89 (s, 1H; pyrrole-H); 4.65 (s, 2H; $-CH_2-$); 2.32 (s, 3H; −CH3); 2.00 (s, 3H; $-CH_3$).

4.9. Synthesis of (4-((bis(pyridin-2-ylmethyl)amino)methyl)phenyl)(3,5-dimethyl-1H-pyrrol-2-yl) methanone (PPMdpa)

Bis(pyridine-2-ylmethyl)amine (dpa, 600 mg, 3 mmol) was dissolved in acetonitrile (20 mL) under nitrogen at room temperature. KI (107 mg, 0.64 mmol) was added with stirring. PPM (605.2 mg, 2.4 mmol) in 25 ml acetonitrile was added slowly from a dropping funnel in 1 h. The reaction was stirred at 80 °C for 8 h. The solvent was removed in vacuum and residue was dissolved in chloroform. The organic layer was washed with water (3 × 50 ml), dried with sodium sulfate and concentrated to give oil liquid after column chromatography on silica gel, dark yellow powder PPMdpa was obtained. Yield: 650 mg (66%); elemental analysis calcd (%) for $C_{26}H_{26}N_4O$: C, 76.07; H, 6.38; N, 13.65. Found: C, 75.76; H, 6.15; N, 13.87. IR (KBr, ν/cm^{-1}): ν = 3251 (=NH), 1596 (C=O), 761 (CH, pyridine). UV–vis (MeOH/nm) ($\varepsilon \times 10^{-4}/dm^3\ mol^{-1}\ cm^{-1}$): 206 ($\varepsilon$ = 2.61), 248 (ε = 1.90), 323 (ε = 2.59). ^1H NMR ($CDCl_3$, 400 MHz, 25 °C, TMS), δ = 9.18 (s, 1H; pyrrole, N–H); 8.54 (d, J = 4.8 Hz, 2H; PyH); 7.70 (td, J = 8.0 Hz, 1.6 Hz, 2H; BzH); 7.60 (t, J = 8.0 Hz, 4H; PyH); 7.51 (d, J = 8.0 Hz, 2H; BzH); 7.17 (dd, ^3J = 6.8 Hz, 5.2 Hz, 2H; PyH); 5.87 (d, J = 2.4 Hz, 1H; pyrrole-H); 3.84 (s, 4H; CH_2-); 3.77 (s, 2H; $-CH_2-$); 2.3 (s, 3H; $-CH_3$); 1.95 (s, 3H; $-CH_3$). ES-MS(ESI^+, MeOH): calcd for $[C_{26}H_{27}N_4O]^+$: 411.15, found 411.36.

4.10. Synthesis of $[(PPMdpa)_2Mn_2(\mu\text{-}Cl)_2Cl_2]_2$ (Mn1)

$MnCl_2 \cdot 4H_2O$ (150 mg, 0.757 mmol) in ethanol (20 mL) was mixed with PPMdpa (250 mg, 0.609 mmol). The mixture was heated to 70 °C for 2 h, and then it was cooled to room temperature. Diethyl ether (20.0 mL) was added to precipitate the products. After filtration, a light yellow solid was obtained. Yield: 251 mg (77%). Elemental analysis calcd. (%) for $C_{26}H_{26}N_4OMnCl_2$: C, 58.21; H, 4.85; N, 10.45. Found: C, 58.03; H, 4.95; N, 10.83. IR (KBr,ν/cm^{-1}): ν = 3239 (=NH), 1610 (C=O), 762 (CH, pyridine). UV–vis(MeOH/nm) ($\varepsilon \times 10^{-4}/dm^3\ mol^{-1}\ cm^{-1}$): 208 ($\varepsilon$ = 2.10), 257 (ε = 1.43), 321 (ε = 1.57).

4.11. Synthesis of $[(PPMdpa)_2Mn_2(\mu\text{-}Ac)_2(Ac)_2]$ (Mn2)

A solution of PPMdpa (84.4 mg, 0.20 mmol) in acetonitrile (10 mL) was mixed with $MnAc_2 \cdot 6H_2O$ (50 mg, 0.2 mmol), and then the mixture was refluxed at 80 °C for 2 h. After the solution was cooled to room temperature, an excess amount of diethyl ether was added, and the obtained yellow brown precipitate was dried under vacuum. Yield: 99 mg (85%). elemental analysis calcd. (%) for $C_{30}H_{32}N_4O_5Mn$: C, 61.75; H, 5.49; N, 9.61. Found: C, 61.86; H, 5.45; N, 9.87. IR(KBr, ν/cm^{-1}): ν = 3264 (=NH), 1606 (C=O), 765 (CH, pyridine). UV–vis(MeOH/nm) ($\varepsilon \times 10^{-4}/dm^3\ mol^{-1}\ cm^{-1}$): 206 ($\varepsilon$ = 2.02), 256 (ε = 1.20), 321 (ε = 1.33).

Acknowledgments

Financial support from National Natural Science Foundation of China (20971059, 21271090) and Coordination Chemistry State key Laboratory Foundation of Nanjing University.

Appendix A. Supplementary data

Supplementary data related to this article can be found at http://dx.doi.org/10.1016/j.ejmech.2014.04.035.

References

[1] G.L. Semenza, Hypoxia-inducible factors: mediators of cancer progression and targets for cancer therapy, Trends in Pharmacological Sciences 33 (2012) 207–214.
[2] V. Mucaj, J.E.S. Sha, M.C. Simon, Effects of hypoxia and HIFs on cancer metabolism, International Journal of Hematology 95 (2012) 464–470.
[3] H. Pelicano, D.S. Martin, R.H. Xu, P. Huang, Glycolysis inhibition for anticancer treatment, Oncogene 25 (2006) 4633–4646.
[4] T.H. Scheuermann, Q.M. Li, H.W. Ma, J. Key, L. Zhang, R. Chen, J.A. Garcia, J. Naidoo, D.E. Frantz, U.K. Tambar, K.H. Gardner, R.K. Bruick, Allosteric inhibition of hypoxia inducible factor-2 with small molecules, Nature Chemical Biology 9 (2013) 271–276.
[5] M.G.V. Heiden, Targeting cancer metabolism: a therapeutic window opens, Nature Reviews Drug Discovery 10 (2011) 672–684.
[6] M. López-Lázaro, The Warburg effect: why and how do cancer cells activate glycolysis in the presence of oxygen? Anti-cancer Agents in Medicinal Chemistry 9 (2009) 517–525.
[7] A. Kohlmann, S.G. Zech, F. Li, T.J. Zhou, R.M. Squillace, L. Commodore, M.T. Greenfield, X.H. Lu, D.P. Miller, W.S. Huang, J.W. Qi, R.M. Thomas, Y.H. Wang, S. Zhang, R. Dodd, S.Y. Liu, R.S. Xu, Y.J. Xu, J.J. Miret, V. Rivera, T. Clackson, W.C. Shakespeare, X.T. Zhu, D.C. Dalgarno, Fragment growing and linking lead to novel nanomolar lactate dehydrogenase inhibitors, Journal of Medicinal Chemistry 56 (2013) 1023–1040.
[8] C. Granchi, S. Roy, C. Giacomelli, M. Macchia, T. Tuccinardi, A. Martinelli, M. Lanza, L. Betti, G. Giannaccini, A. Lucacchini, N. Funel, L.G. Leon, E. Giovannetti, G.J. Peters, R. Palchaudhuri, E.C. Calvaresi, P.J. Hergenrother, F. Minutolo, Discovery of N-hydroxyindole-based inhibitors of human lactate dehydrogenase isoform A (LDH-A) as starvation agents against cancer cells, Journal of Medicinal Chemistry 54 (2011) 1599–1612.
[9] R.A. Ward, C. Brassington, A.L. Breeze, A. Caputo, S. Critchlow, G. Davies, L. Goodwin, G. Hassall, R. Greenwood, G.A. Holdgate, M. Mrosek, R.A. Norman, S. Pearson, J. Tart, J.A. Tucker, M. Vogtherr, D. Whittaker, J. Wingfield, J. Winter, K. Hudson, Design and synthesis of novel lactate dehydrogenase A inhibitors by fragment-based lead generation, Journal of Medicinal Chemistry 55 (2012) 3285–3306.
[10] J.Q. Chen, J. Russo, Dysregulation of glucose transport, glycolysis, TCA cycle and glutaminolysis by oncogenes and tumor suppressors in cancer cells, Biochimica et Biophysica Acta 1826 (2012) 370–384.
[11] V. Gogvadze, B. Zhivotovsky, S. Orrenius, The Warburg effect and mitochondrial stability in cancer cells, Molecular Aspects of Medicine 31 (2010) 60–74.
[12] M. López-Lázaro, A new view of carcinogenesis and an alternative approach to cancer therapy, Molecular medicine. [Molecular Medicine (Cambridge, Mass.)] 16 (2010) 144–153.
[13] M. López-Lázaro, Dual role of hydrogen peroxide in cancer: possible relevance to cancer chemoprevention and therapy, Cancer Letters 252 (2007) 1–8.
[14] D.A. Stoyanovsky, Z.H. Huang, J.F. Jiang, N.A. Belikova, V. Tyurin, M.W. Epperly, J.S. Greenberger, H. Bayir, V.E. Kagan, A manganese-porphyrin complex decomposes H_2O_2, inhibits apoptosis, and acts as a radiation mitigator in vivo, ACS Medicinal Chemistry Letters 2 (2011) 814–817.
[15] D.F. Zhou, Q.Y. Chen, Y. Qi, H.J. Fu, Z. Li, K.D. Zhao, J. Gao, Anticancer activity, attenuation on the absorption of calcium in mitochondria and catalase activity for manganese complexes of N-substituted di(picolyl)amine, Inorganic Chemistry 50 (2011) 6929–6937.
[16] X. Yang, Q.Y. Chen, M.Y. Kong, L.L. Qu, Z.R. Geng, Z.L. Wang, An ionic liquid-modified nano-vehicle to construct nano-models of catalase to target mitochondria, Journal of Materials Chemistry 22 (2012) 20304–22209.
[17] Q.Y. Chen, D.F. Zhou, J. Huang, W.J. Guo, J. Gao, Synthesis, anticancer activities, interaction with DNA and mitochondria of manganese complexes, Journal of Inorganic Biochemistry 104 (2010) 1141–1147.
[18] G. Anderegg, N.G. Podder, P. Blaeuenstein, M. Hangartner, H. Stuenzi, Pyridine derivatives as complexing agents X. Thermodynamics of complex formation of N,N'-bis-(2-pyridylmethyl)-ethylenediamine and of two higher homologues, Journal of Coordination Chemistry 4 (1975) 267–275.
[19] Q.Y. Chen, J. Huang, W.J. Guo, J. Gao, Synthesis, characterization, DNA interaction and cytotoxic activities of copper complexes with ethyl 2-[bis(2-pyridylmethyl)amino]propionate, Spectrochimica Acta A: Molecular and Biomolecular 72 (2009) 648–653.
[20] A. Mai, S. Massa, R. Ragno, I. Cerbara, F. Jesacher, P. Loidl, G. Brosch, 3-(4-Aroyl-1-methyl-1H-2-pyrrolyl)-N-hydroxy-2-alkylamides as a new class of synthetic histone deacetylase inhibitors. 1. Design, synthesis, biological evaluation, and binding mode studies performed through three different docking procedures, Journal of Medicinal Chemistry 46 (2003) 512–524.
[21] S.K. Shakhatreh, E.G. Bakalbassis, C.A. Tsipis, A.P. Bozopoulos, D.W. Dreissig, H. Hartl, Strong ferromagnetism between copper (II) ions separated by 6.7. ANG. in a new phthalato-bridged copper (II) binuclear complex, Inorganic Chemistry 30 (1991) 2801–2806.
[22] I. Romero, L. Dubois, M.N. Collomb, A. Deronzier, J.M. Latour, J.A. Pécaut, A dinuclear manganese(II) complex with the $\{Mn_2(\mu\text{-}O_2CCH_3)_3\}^+$ core: synthesis, structure, characterization, electroinduced transformation, and catalase-like activity, Inorganic Chemistry 41 (2002) 1795–1806.
[23] B.K. Shin, M.Y. Kim, J.H. Han, Hydrogen peroxide disproportionation by the $[TPA_2Mn_2(\mu\text{-}Cl)_2]^{2+}$ complex, Polyhedron 29 (2010) 2560–2568.
[24] J.N. Weiss, The Hill equation revisited: uses and misuses, FASEB Journal: Official Publication of the Federation of American Societies for Experimental Biology 11 (1997) 835–841.
[25] B.K. Shin, M.Y. Kim, J.H. Han, Synthesis, structure and catalase activity of the $[TPA2Mn2(\mu\text{-}Cl)2]^{2+}$ complex, Polyhedron 26 (2007) 4557–4566.
[26] M.U. Triller, W.Y. Hsieh, V.L. Pecoraro, A. Rompel, B. Krebs, Preparation of highly efficient manganese catalase mimics, Inorganic Chemistry 41 (2002) 5544–5554.
[27] S. Groni, P. Dorlet, G. Blain, S. Bourcler, R. Guillot, E. Anxolabehere-Mallart, Reactivity of an aminopyridine $[LMn^{II}]^{2+}$ Complex with H_2O_2. Detection of intermediates at low temperature, Inorganic Chemistry 47 (2008) 3166–3172.
[28] M. Shank, V. Barynim, G.C. Dismukes, Protein coordination to manganese determines the high catalytic rate of dimanganese catalases. Comparison to functional catalase mimics, Biochem 33 (1994) 15433–15436.
[29] W.F.J. Beyer, I. Fridovich, Pseudocatalase from *Lactobacillus plantarum*: evidence for a homopentameric structure containing two atoms of manganese per subunit, Biochem 24 (1985) 6460–6467.
[30] N. Dehne, G. Hintereder, B. Brüne, High glucose concentration attenuate hypoxia-inducible factor-1α expression and signaling in non-tumor cells, Experimental Cell Research 316 (2010) 1179–1189.
[31] N. God, M. Kanai, Hopoxia-inducible factors and their roles in energy metabolism, International Journal of Hematology 95 (2012) 457–463.
[32] G.M. Sheldrick, SHELXL-97, Program for the Refinement of Crystal Structures, University of Gőttingen, Gőtingen, 1997.
[33] M. Dixon, The determination of enzyme inhibitor constants, The Biochemical Journal 55 (1953) 170–171.